NOTES AND CORRESPONDENCE

A Small Portable Mie–Rayleigh Lidar System to Measure Aerosol Optical and Spatial Properties*

J. N. PORTER, B. R. LIENERT, S. K. SHARMA, AND H. W. HUBBLE

Hawaii Institute of Geophysics and Planetology, University of Hawaii at Manoa, Honolulu, Hawaii

5 December 2001 and 8 May 2002

ABSTRACT

The characteristics of a small, lightweight portable lidar system for measuring aerosol (Mie) scatter at wavelengths of 1064 and 532 nm are described. It uses a 20-Hz Nd:YAG pulsed laser as a source and a 12.7-cm-diameter telescope as a receiver. By using a minimal number of commercially available components, the cost of construction has been reduced. The lidar has a useable range of 60–3000 m for clean marine conditions. Its performance has been demonstrated using measurements of tropospheric aerosols on the island of Hawaii.

1. Introduction

Atmospheric lidars have been used in a variety of areas, such as mapping aerosol, water vapor, and other trace species (Stephens 1994; Sharma et al. 2001). While many lidar systems require a dedicated trailer, several smaller lidar systems, such as the micropulse lidar (Spinhirne et al. 1995; Welton et al. 2000), the Vaisala CT25K ceilometer (details online at http://info.nies.go.jp:8094/AsiaNet/nies/home/amami-ceilo/), and the Los Alamos lidar (Cooper and Eichinger 1994), are small enough to be deployed by one or two people. Here we report on a new small lidar system that we have developed using mainly off-the-shelf components. The system is described and an example from a field experiment is given.

2. Lidar design

Several approaches can be taken in designing a small lidar system. For instance, both the micropulse and the Vaisala lidars have low energies per pulse (microjoules per pulse) and high repetition rates, which allows them to be eye-safe systems. This eye safety design and the fact that they are enclosed in weatherproof housings means that they can be deployed unattended. A disadvantage of these systems is that they require more time to collect data with good signal to noise (up to 1 min). A different approach, which we employ, is to use a laser with higher energies per pulse (millijoules per pulse) but lower laser repetition rates. A similar approach is used by the Los Alamos laser system (Cooper and Eichinger 1994). The disadvantage of this approach is that the lidar is not eye safe, and an operator must always be present to shut the system off whenever an aircraft, ship, or person comes into range. Therefore, these systems are typically not designed to be weatherproof. On the other hand, their advantage lies in the fact that they can collect data with good signal to noise in seconds (or less), making rapid scanning possible.

Our lidar system (shown in Figs. 1 and 2) follows a simple design and includes relatively few components. The lidar is based on a 12.7-cm-diameter telescope (Meade ETX125) that is mounted on a two-axis scanning motor. The laser (Big Sky Laser, Ultra CFR Nd:YAG) is a 20-Hz pulsed system with 20-mJ energy at 1064 nm, 12-mJ at 532 nm, and 7-mJ at 355 nm. The laser beam diameter is ~3 mm and it has a divergence of 1 mrad at 532 nm and 1.5 mrad at 1064 nm. The laser is mounted on the side of the telescope and two small prisms are used to bring the beam to the center of the telescope to make it a coaxial system. Shielding tubes are used along the path of the laser beam to prevent stray light from saturating the detector. No beam expander is used, but divergence of the beam causes it to be 4 m in diameter at 1-km distance. The final prism has three adjusting screws, which allows the laser beam to be aligned along the telescope's optical axis. A beam splitter is used to separate the telescope output into

* School of Ocean and Earth Science and Technology Contribution Number 5975.

Corresponding author address: Dr. John N. Porter, University of Hawaii, 2525 Correa Road #131, Honolulu, HI 96822.
E-mail: johnport@hawaii.edu

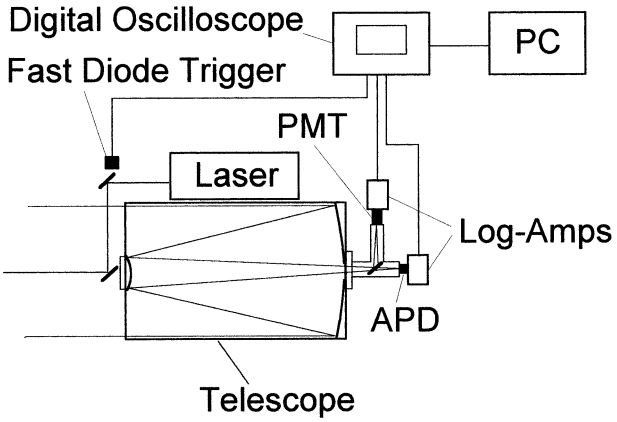

FIG. 1. Schematic of the portable lidar system.

1064- and 532-nm components. A small Hamamatsu H6779 photo multiplier tube (PMT), located at the focal point of the telescope, detects the 532-nm backscatter signal, while an EG&G C3095 avalanche photodiode (APD) detects the 1064-nm backscatter signal. The PMT detector has a detector area with a 6-mm diameter. The APD detector is quite small (1 mm), so a 2.5-cm-diameter aspheric lens is used to increase the effective diameter of the APD by a factor of 10. Barr interference filters (3-nm bandwidth) in front of each detector are used to reject background light at other wavelengths. The PMT and APD signals are amplified by custom-built logarithmic amplifiers (Lienert et al. 2002) that increase the dynamic range and decrease the digitization accuracy requirements. Digitization is performed with a Tektronics TDS3014 8-bit digital oscilloscope, with the output supplied to a laptop computer via a serial link. When the oscilloscope is set to averaging (which we do), the data are saved and transferred to the computer as 16-bit numbers, although it is not expected that these numbers are better than 10-bit quality, considering they were originally digitized at 8-bit resolution. The data are processed and displayed in real time on a laptop computer using custom software. In order to trigger the oscilloscope, a portion of the laser light (532 nm) is collected with an optical fiber at one of the turning prisms and brought to a fast photodiode. The signal from the photodiode provides the oscilloscope trigger. This signal is also used to normalize the lidar signal correcting for variations in laser power. With the current analog to digital configuration, the system collects backscatter lidar signal with good signal to noise out to 3-km range (or farther, depending on the aerosol loading) in 3 s. It takes 4 s to transfer the data from the oscilloscope to the computer. Scattering from clouds has been measured out to a 9-km range.

The near-field attenuation effect (overlap factor), caused by the telescope central obstruction (Halldorsson and Langerholc 1978), causes the initial peak in the backscattered signal to appear at 30-m range. This near-field effect occurs at a relatively short range in our lidar system because we do not use an aperture and the detector size is the effective aperture (6-mm diameter). In processing the data we typically begin at 60-m range, where no noticeable near-field effect occurs in the inverted lidar data.

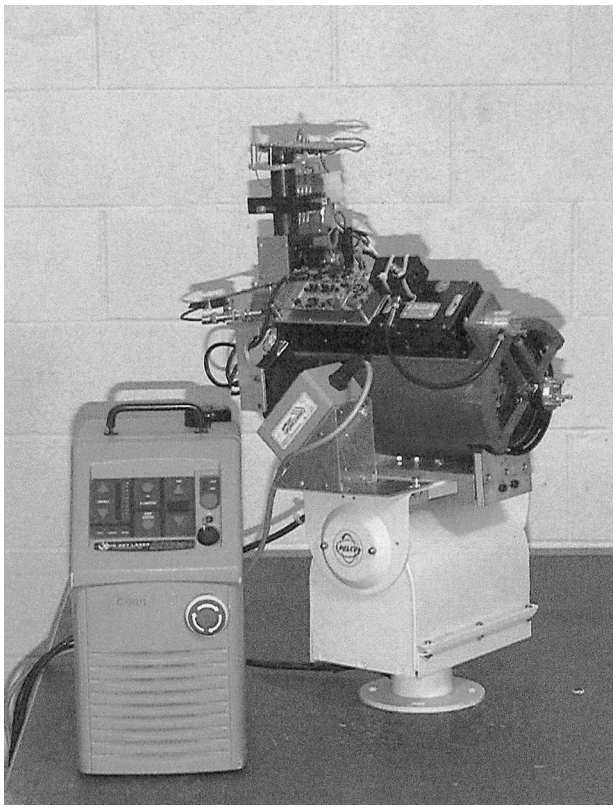

FIG. 2. Photograph of the portable lidar system with the laser power supply.

Alignment and focus of the system is relatively straightforward if certain procedures are followed. The first step is to set the telescope field of view and get the laser aligned with the telescope. To do this we remove the detector and apply a light source at the same position at which the detector was located. For this step we use a fiber-optic cable connected to a red He:Ne laser. At night the red light coming out of the telescope is pointed at a wall 30 m away. By adjusting the focus and measuring the beam diameter at several distances, the telescope beam divergence is set to 2 mrad, which is slightly larger than the system laser beam divergence (4 mrad). Since the detector is 6 mm in diameter, instead of the 1-mm fiber the telescope–detector system actually has an acceptance angle that is much larger. Next the main lidar's laser is turned on and the position of the lidar beam (small green spot) is adjusted until it falls within the center of the large red spot. At this point the detector is placed back into its position. This simple procedure aligns the system and no further alignment is needed.

If the lidar is already roughly aligned then it is possible to use two different approaches to align the laser.

One is to point the lidar at a hard target and use an eyepiece (at the detector position) to see scattered laser light. If the laser light does not appear in the center of the eyepiece, then the laser must be aligned. This approach offers the advantages that it can be done in the day and the target can be farther away. The disadvantage of this approach is that the laser must already be fairly well aligned to be seen in the eyepiece. Alternatively, it is possible to simply maximize the detector signal, as seen on an oscilloscope, at a distant point using atmospheric signal. We have also used an island as a distant target (9 km away) but find the island signal is more variable than a simple atmosphere signal, possibly due to atmospheric small-scale refraction effects. In using this last approach it is advisable to go back to the eyepiece approach as a final check because it is possible to completely misalign the system if one is not careful.

Misalignment of the laser will also appear in the final data processing. If the lidar is misaligned, then at some point the lidar signal does not continue to decrease but remains constant with range (time). Porter et al. (2000) showed that in using the forward stepping approach to derive the aerosol scattering coefficient, an incorrect phase function or lidar calibration causes the derived aerosol extinction values to become either too large or small at the more distant ranges. But if the raw lidar data are constant with range, as would be the case for a misaligned lidar, then using an incorrect value for the phase function or lidar calibration does not cause the inverted aerosol extinction values to blow up systematically with range (only the noise increases, without any trend). This failure to blow up when using an incorrect lidar calibration or phase function value is a sure sign that the system is misaligned.

3. Lidar measurements

Lidar measurements were made on 17 August 2001 on the east side of the Big Island of Hawaii on the Chain of Craters road. This region is just south of the Kilauea lava flows. At this location the northeast trade winds come over the land briefly before turning south and becoming roughly parallel to the coastline. On this day the sky was cloud free, which is fairly unusual for Hawaii and suggests that strong subsidence was occurring. After about 1100 LT a band of isolated small clouds began forming near the coastline where a low-level sea breeze was developing. At this time we also observed that the clouds and the volcano plume (farther inland) were moving parallel to the coast (northeast wind), while the low-level surface winds were onshore (southeast wind). The low-level sea breeze was serving as a trigger to initiate small isolated clouds near the coastline.

Figure 3 shows raw data from the lidar logarithmic amplifier (log amp) output (from the PMT at 532 nm) plotted versus time that was collected on the Big Island of Hawaii on 17 August 2001. The custom log amp has

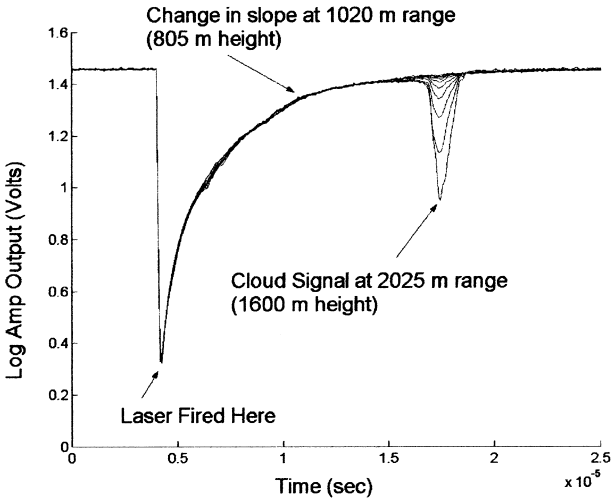

FIG. 3. Ten lidar traces, showing the scattered signal as a function of range as it appears out of our log map. The lidar was pointed vertically, with an elevation of 52°.

a built-in offset so that the idle voltage output is greater than zero (Lienert et al. 2001). On this occasion, the lidar was pointing at 53° elevation. Figure 3 shows 10 different 100-shot lidar stacks (collected sequentially), which depict the change in the lidar log amp output as the vehicle passed under a cloud based at 2000-m altitude (the last cloud shown in Fig. 4). A distinct change in the output slope can also be seen at the 1020-m range, suggesting a change in aerosol scatter.

Figure 4 shows the aerosol scattering coefficients derived from the lidar measurements collected at this time. The inversion approach is discussed below. High aerosol scatter occurs near the surface, and relatively high aerosol scatter existed up to ~800 m, with clean air above 800 m. Evidence of thermals with trails of higher aerosol scatter are seen feeding into small clouds at ~1600 m height. The high aerosol scattering concentrations seen in the lowest 200 m are likely due to sea salt spray (which was observed) or possibly from low amounts of volcanic emissions from farther up the coast. The main part of the plume (from the Kilauea vent) was aloft and passed southwest of this site. The Hilo sounding (collected by the National Weather Service) for this day (Fig. 5) was collected 2 h after the lidar measurements and about 35 miles north of our lidar measurements. Despite these time and space differences, many similar features appear in the lidar and sounding datasets. Near the surface the sounding shows a surface layer, which is also present in the aerosol scattering concentrations. From ~200 to 800 m the sounding gives a hint of a mixed layer, which is consistent with the intermediate aerosol scattering values seen in that layer. From ~800 to 1600 m the sounding suggests a transition layer with no cloud layer present. Adiabatic lifting of surface parcels suggests that the cloud base should be near 1450 m (Wallace and Hobbs 1977), but there is little if any

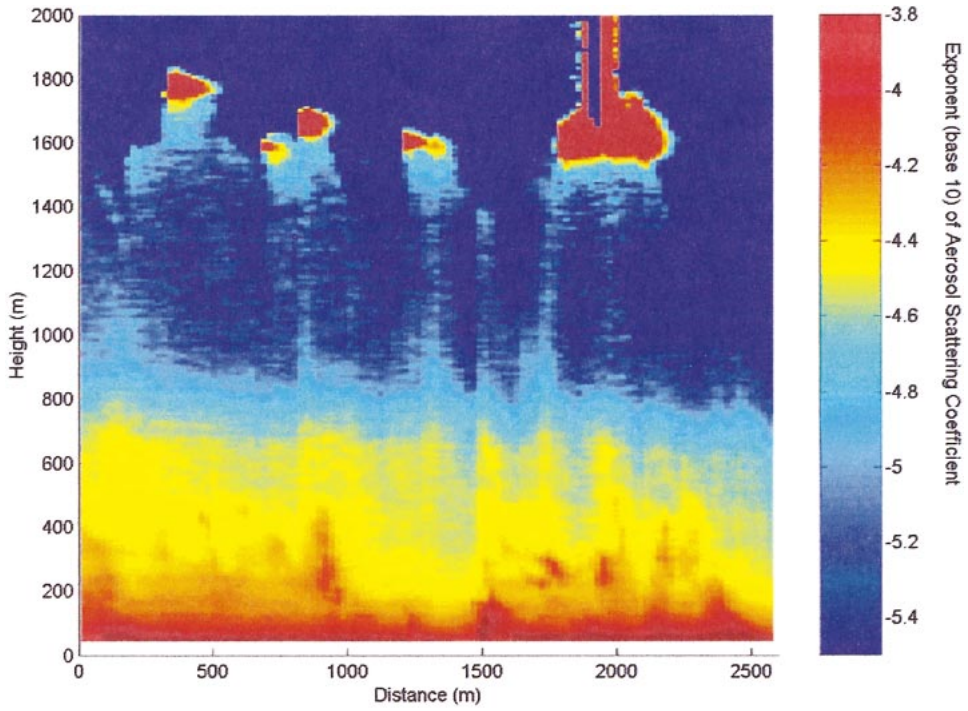

FIG. 4. Image of aerosol scattering coefficient (532 nm) derived from the little lidar measurements on the southeast side of Hawaii on 17 Aug 2001. The color bar shows the exponent (base 10) of the aerosol scattering coefficient (i.e., -4 is 10^{-4} m^{-1}).

indication of a cloud layer in the sounding. At the lidar site only small clouds were observed and only along the coastline. The cloud base and tops are only slightly higher than what the sounding predicts. Overall the agreement between the sounding and lidar datasets is good. Although models have been developed to predict the structure of the trade wind mixed layer (Albretch 1984), these models remain poorly validated. The use of sounding and lidar datasets can provide unique information about the atmospheric boundary layer structure.

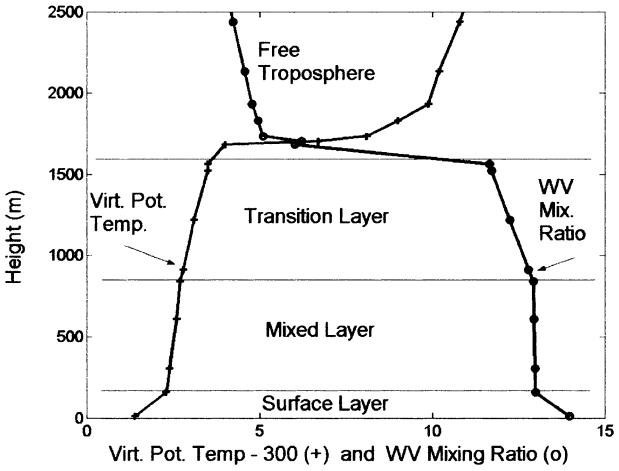

FIG. 5. Atmospheric sounding taken at Hilo, Hawaii, at 1400 LT 19 Aug 2001. A value of 300 has been subtracted from the virtual potential temperature to fit on the same scale.

4. Lidar data inversion

Following Reagan (1995) or Porter et al. (2000), the lidar equation can be written as

$$n(r) = \frac{C\beta(r)T(r)^2}{r^2}, \tag{1}$$

where $n(r)$ is the number of photons from distance r, C is the lidar calibration, $\beta(r)$ is the backscattering coefficient (m^{-1} sr^{-1}) at range r, and $T(r)^2$ is the two-way transmission given by $T(r)^2 = e^{-2\int \sigma_e(r)\,dr}$ where $\sigma_e(r)$ is the extinction coefficient (m^{-1}) at range r. The backscattering coefficient is given by $\beta(r) = [P_m(r)\sigma_m(r) + P_a(r)\sigma_a(r)]/(4\pi)$, where $P_m(r)$ and $P_a(r)$ are the molecular and aerosol phase function at 180° scattering angle (at range r), and $\sigma_m(r)$ and $\sigma_a(r)$ are molecular and aerosol scattering coefficients (m^{-1}) at range r. For the clean marine atmosphere the absorption is negligible, so we assume that the extinction coefficient is the sum of the molecular and aerosol scattering coefficients: $\sigma_e(r) = \sigma_m(r) + \sigma_a(r)$. In using Eq. (1) to estimate the aerosol scattering coefficient the uncertainties lie in the lidar calibration, C, and in the backscattering coefficient, $\beta(r)$. Because the aerosol phase function $P_a(r)$ is unknown, $\beta(r)$ is unknown. But from Eq. (1) it can be seen that the two unknowns, C and $\beta(r)$, form a product

so that there is really only one unknown. Also, it can be seen that an error in C can be corrected by an error in $\beta(r)$ and visa versa.

Sun photometer measurements of aerosol optical depths can provide independent data to constrain the inversion of aerosol extinction coefficients from lidar data. Several different approaches have been used in carrying out this effort (Welton et al. 2000). The approach we have used is to make a best guess at the aerosol phase function and manually adjust the lidar calibration until the integrated optical depth derived from the lidar agrees with coincident sun photometer measurements. A constant phase function value of 0.5 was used as representative of marine aerosol under moderate wind speeds (Porter et al. 2000). The processing of the lidar data was carried out with a simple forward stepping approach (Porter et al. 2000, 2001a), accounting for the change of molecular scatter with height. The aerosol sun photometer measurements used to constrain the inversion of the lidar data were obtained with a MICROTOPS hand-held sun photometer (manufactured by Solar Light Co., Inc.; Porter et al. 2001b) and had an average value of 0.06 at 500 nm. An aerosol optical depth of 0.015 was measured at the nearby Mauna Loa Observatory and was subtracted from our measurements as a free troposphere background contribution, resulting in an aerosol optical depth of 0.045 for the boundary layer. This inversion approach forces the lidar-derived integrated aerosol optical depth to be the same as the sun photometer optical depth. While this means that the overall aerosol scattering coefficient values are correct, on smaller scales they can be off due to variability in the aerosol size distribution.

5. Conclusions

Here we describe a small low-cost portable lidar, which is being used for studies of atmospheric structure and aerosol dispersion. The system has been used in the field to provide information on the atmospheric stability and aerosol structure. Studies of atmospheric structure and aerosol dispersion are often based on sounding datasets alone. Small portable lidars can offer additional information on the mixing processes from which further insight can be obtained (Cooper and Eichinger 1994).

Acknowledgments. This effort has been supported in part by NASA Grants NAG5-6340 and NAG5-7139, and ONR Grant N00014-96-1-0317. We also wish to thank Manash Ghosh for assistance in field measurements.

REFERENCES

Albretch, B., 1984: A model study of downstream variations of the thermodynamic structure of the trade winds. *Tellus,* **36A,** 187–202.

Cooper, D. I., and W. E. Eichinger, 1994: Structure of the atmosphere in an urban planetary boundary layer from lidar and radiosonde observations. *J. Geophys. Res.,* **99** (D11), 22 937–22 948.

Halldorsson, T., and J. Langerholc, 1978: Geometrical form factors for the lidar function. *Appl. Opt.,* **17,** 240–244.

Lienert, B., J. N. Porter, N. Ahlquist, D. Harris, and S. Sharma, 2002: A 50-MHz logarithmic amplifier for use in lidar measurements. *J. Atmos. Oceanic Technol.,* **19,** 654–657.

Porter, J. N., B. Lienert, and S. K. Sharma, 2000: Using the horizontal and slant lidar calibration methods to obtain aerosol scattering coefficients from a coastal lidar in Hawaii. *J. Atmos. Oceanic Technol.,* **17,** 1445–1454.

——, S. K. Sharma, and B. R. Lienert, 2001a: Obtaining calibrated marine aerosol extinction measurements using horizontal lidar measurements, differential lidar-target measurements and a polar nephelometer. *Proc. SPIE Meeting on Lidar Remote Sensing for Industry and Environment Monitoring,* Sendai, Japan, SPIE, 274–281.

——, M. Miller, C. Pietras, and C. Motell, 2001b: Ship-based sun photometer measurements using Microtops sun photometers. *J. Atmos. Oceanic Technol.,* **18,** 765–774.

Reagan, J. A., 1995: New generation lidars to support aerosol radiation/climate forcing studies. *Proc. IGARSS95,* Florence, Italy, IEEE, 2313–2315.

Sharma, S. K., B. R. Lienert, and J. N. Porter, 2001: Scanning lidar measurements of marine aerosol fields at a coastal lidar site in Hawaii. *Proc. SPIE Meeting on Lidar Remote Sensing for Industry and Environment Monitoring,* Sendai, Japan, SPIE, 159–166.

Spinhirne, J. D., J. A. R. Rall, and V. S. Scott, 1995: Compact eye safe lidar systems. *Rev. Laser Eng.,* **23,** 112–118.

Stephens, G. L., 1994: *Remote Sensing of the Lower Atmosphere: An Introduction.* Oxford University Press, 523 pp.

Wallace, J. M., and P. V. Hobbs, 1977: *Atmospheric Science: An Introductory Survey.* Academic Press, 467 pp.

Welton, E. J., and Coauthors, 2000: Ground-based lidar measurements of aerosols during ACE-2: Instrument description, results, and comparisons with other ground-based and airborne measurements. *Tellus,* **52B,** 635–650.